ASSESSMENT OF A THREE-DIMENSIONAL FIBER ORIENTATION MODEL FOR TIMBER

*M. Hu**†*

PhD student
E-mail: min.hu@lnu.se

A. Olsson

Professor
E-mail: anders.olsson@lnu.se

M. Johansson

Professor
E-mail: marie.johansson@lnu.se

J. Oscarsson

University Lecturer
Department of Building Technology
Linnaeus University, Växjö, Sweden
E-mail: jan.oscarsson@lnu.se

E. Serrano

Professor
Division of Structural Mechanics
Lund University, Lund, Sweden
E-mail: erik.serrano@construction.lth.se

(Received November 2015)

Abstract. Wood is an orthotropic material with very different properties along and across fibers, and every board has its own pattern of knots and fiber deviations. Therefore, detailed knowledge of the three-dimensional (3D) fiber orientation of individual boards would enable more accurate assessment of properties such as stiffness, strength, and shape stability. This paper presents a method for modeling 3D fiber orientation of side boards of Norway spruce. The method is based on dot laser scanning and utilization of the tracheid effect, and it is verified by a comparison between strain fields calculated on the basis of the fiber orientation model and corresponding strains determined using digital image correlation (DIC) technique. By means of the method, it is possible to identify knots and to reproduce the fiber orientation in clear wood in the vicinity of knots. Fiber orientation models of side boards including traversing edge knots were established and integrated in finite element models of boards used for simulation of four-point bending tests. The same boards were also tested in laboratory and displacement fields of the wide faces were recorded at different load levels using DIC technique. Comparisons of strain fields from measurements and simulations showed close agreement, regarding both strain patterns and strain levels. Local strain concentrations caused by very small defects were detected using the models and also found from the laboratory test results. The modeling approach may be used both to achieve improved accuracy of existing machine strength grading methods and, after further development, also for more advanced analysis of eg crack propagation and strength of timber

Keywords: Diving angle, fiber angle, grain angle, laser scanning, strength grading, tracheid effect.

* Corresponding author
† SWST member

INTRODUCTION

Background

Strength and other mechanical properties of timber are to a large extent dependent on the occurrence of knots and the surrounding local fiber orientation (Johansson 2003). Therefore, detailed knowledge of these properties should enable accurate prediction of strength. Today industry laser scanners, operating in a speed corresponding to the production speed in sawmills, collect high-resolution data regarding local fiber orientation on timber surfaces. Therefore, research should aim at 1) the establishment of detailed models of timber including local fiber orientation on the basis of information from laser scanning and 2) accurate prediction of timber strength on the basis of such models. The overall objective of this paper is to contribute regarding the first of these aims, ie toward detailed models of timber boards established on the basis of information from scanning. A brief overview of empirical models that have been suggested in the past regarding fiber orientation in the vicinity of knots, and a review of a recently developed machine strength grading method that rely on knowledge of local fiber orientation are given below, followed by an account of the specific objectives of the present paper.

Fiber Orientation Around Knots—Models Suggested in the Past

Serious attempts to describe fiber orientation around knots have been made at least since the 1970s. Goodman and Bodig (1978) suggested a model based on a grain-flow analogy, motivated by the visual similarity between the grain pattern within a growth layer of a tree in the vicinity of a knot and the streamline pattern of a fluid passing around an elliptical obstacle. Hence, the suggested model was based on stream functions to describe the grain deviation due to a knot in the longitudinal-tangential plane of the wood material. This two dimensional grain-flow analogy was adopted and further developed by Foley (2001, 2003) who developed a three-dimensional (3D) paradigm of local material directions. In Foley's model, the fiber orientation in the longitudinal-tangential plane of a growth layer was modeled by the grain-flow analogy, whereas the fiber orientation in the longitudinal-radial plane was determined based on mathematical functions describing the observed geometry of growth layers in the vicinity of knots. Another starting point for describing the fiber course around knots is a principal stress-based logic put forward by Mattheck (1998). The basic idea is that fibers around a knot are orientated in the directions of principal stresses due to natural loads during the growth of the tree. An initial stress analysis, in which isotropic material properties are assumed, is first performed. Then follows an iterative procedure where the orientation of fibers in each position follows the direction of the major principal stress in the same position according to the previous calculation. Thus from the second step forward in the calculation, an orthotropic material model is employed. The iterative process is terminated when the directions of principal stresses no longer change significantly from one step to the next. The direction of the major principal stress in each position of the last step thus indicates the fiber orientation in that position within the tree. The grain-flow analogy, Foley's model, and the principal stress-based model are frequently referred to and applied to models of timber. Cramer and Goodman (1983) adopted the grain-flow analogy and applied the resulting fiber course in finite element (FE) models of wooden boards for stress analysis and strength prediction. In more recent years, Lang and Kaliske (2013) discussed and compared the grain-flow analogy and the principal stress-based model. They showed that the two models provide similar results regarding the fiber orientation around knots. On the basis of work by Hackspiel (2010), Lukacevic and Füssl (2014) presented an FE model of timber in which Foley's model was employed to establish a 3D fiber course around knots. The model was used to estimate effective stiffness and strength properties, and was subjected to experimental verification, which showed promising results.

Though the models mentioned above in this section provide reasonable results regarding fiber orientation, they are all dependent on information of size and location of the knots within the piece of timber to be examined. Hence, without such information these cannot be used for grading purposes.

Laser Scanning and the Tracheid Effect

Since about 20 yr, industry scanners able to determine the in-plane fiber orientation on timber surfaces with a resolution of a few millimeters have been available. This is done by using the so-called "tracheid effect", which means that when softwood surfaces are illuminated by laser rays the light spread more along fibers than across (Matthews and Beech 1976; Soest et al 1993). Thus the light spots on the wood surface become elliptical, rather than circular in shape and the major axis of the elliptically shaped light spot indicate the fiber direction in the plane of the surface. Figure 1 shows 1) the surface of a piece of wood including a knot, 2) spread of laser light on the wood surface, 3) enlargement of one of the laser dots in which the length and direction of the main axes are marked out, and 4) the identified in-plane fiber orientation of the wood surface. Note that a light spot that illuminates a surface on the knot surface does not show an elliptical shape as pronounced as a light spot on a clear wood surface does. Therefore, in the knot area, where the ratio between the identified major and minor axes of light spots are close to one, the lines in Fig 1d representing the in-plane fiber orientation are drawn with dashed lines rather than with solid lines. The lines drawn in Fig 1d thus represent the in-plane fiber orientation but, of course, in reality there is also an out of plane component, ie a "diving angle" between the wood surface and the fibers. Simonaho et al (2004) showed that for Scots pine (*Pinus sylvestris* L.) and silver birch (*Betula pubescens*) the tracheid effect can also be used for determination of the diving angle by considering the ratio between the length of the minor and major axes of the elliptically shaped light spot on the wood surface, ie the diving angle increases as the value of this ratio approaches one. In their research, they suggested a mapping between this ratio and the diving angle, which was established on the basis of experimental data of the two species.

Strength Grading Based on Data of Fiber Orientation

As discussed above in *Background* section, knowledge of fiber orientation should enable accurate predictions of strength but until recently fiber orientation data have not been used for strength grading purposes. Olsson et al (2013) presented, however, a new method for strength grading of sawn timber based on a combination of laser

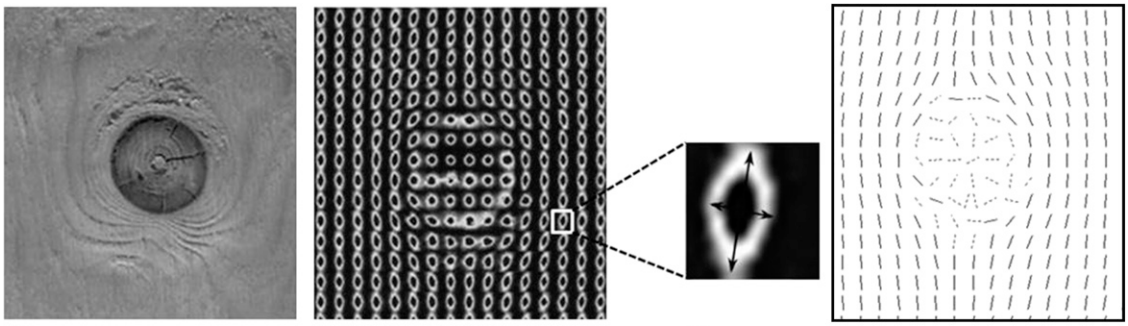

Figure 1. (a) The surface of a piece of wood including a knot, (b) spread of dot laser light on the wood surface, (c) enlargement of one of the laser dots in which the length and direction of the main axes are marked out, and (d) the identified in-plane fiber orientation of the wood surface (images a-b originate from Petersson 2010).

scanning, dynamic excitation, and weighing of boards, where the novelty lay in using fiber orientation information from laser scanning. In this method, the scanning of face and edge surfaces is performed using a scanner of make WoodEye®, (from WoodEye AB, Linköping, Sweden) equipped with four sets of multisensor cameras and dot lasers making use of the tracheid effect. Using, in addition to the determined in-plane fiber orientation, common relationships between MOE in fiber direction and MOE in across fiber direction, the local MOE in the direction of the board is calculated. This in turn is used to calculate, by integration over the board cross section, the bending stiffness locally of a segment along the board. Figure 2 illustrates 1) local fiber directions determined on a wood surface, 2) cross section divided into subareas implying that the exhibited angle φ and corresponding MOE in the member's longitudinal direction is valid within the volume $dA \times dx$, 3) distribution of longitudinal MOE around the exhibited knot, and 4) segment of length dx. The edgewise bending stiffness of this segment is calculated by stiffness integration over the segment's cross section. A new indicating property (IP) to bending strength was, thus, defined based on the lowest calculated edgewise bending stiffness along the board.

An initial type testing procedure, see the European Standard EN 14081-2 (2010 +A1:2012), was performed and in March 2015 the method was approved by the task group TG1 established under the technical committee TC 124 within the European Committee for Standardization (approval process described in Olsson and Oscarsson 2016). Consequently, the method is now available on the market. By means of the suggested IP of the new method, it is possible to predict the bending strength with high accuracy. On a sample consisting of more than 900 boards of Norway spruce (*Picea abies* [L.] Karst.) of various dimensions, the coefficient of determination between the bending strength and the new IP was $R^2 = 0.69$. For comparison, the R^2 value

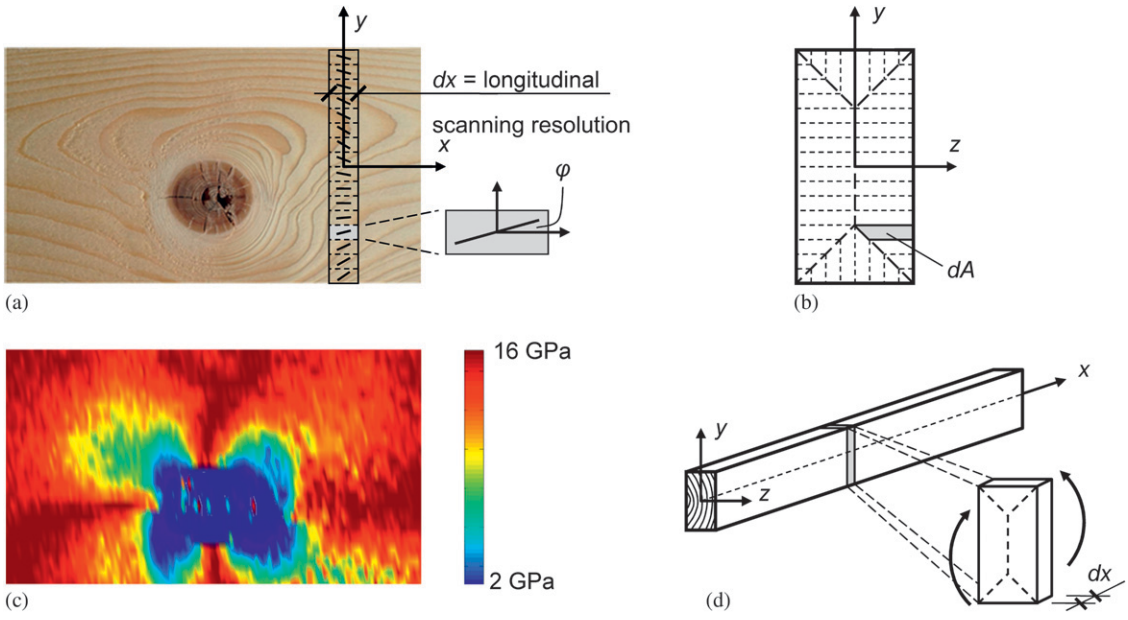

Figure 2. (a) Local fiber directions scanned on a member's surface by means of a row of laser dots, (b) cross section divided into subareas implying that the exhibited angle φ and corresponding MOE in the member's longitudinal direction is valid within the volume $dA \times dx$, (c) distribution of longitudinal MOE around the exhibited knot, and (d) segment of length dx. The edgewise bending MOE of this segment is calculated by stiffness integration over the segment's cross section.

obtained for bending strength vs dynamic longitudinal MOE was only 0.53 for the same sample.

The new grading method is based on several simplifying assumptions regarding fiber orientation. First, it is assumed that fibers are oriented in the plane of the investigated surface, ie the diving angle is ignored. Second, it is assumed that the fiber orientation determined on the surface is representative to a certain depth into the board (Fig 2b). In reality, however, the orientation inside the timber is not identical to the one on the surface but depends on the occurrence and orientation of knots (eg Foley 2003). Thus, a rather crude fiber orientation model was used as a basis for this strength grading method and it is reasonable to assume that a more accurate fiber orientation model, namely one that makes better use of the data from scanning and combines it with general knowledge of the fiber orientation in the vicinity of knots, would enable even better machine strength grading methods. Hence, more research and development in this field is motivated.

Olsson and Oscarsson (2014) presented research on identification of the diving angle using the same kind of mapping as suggested by Simonaho et al (2004), but calibrated the relationship for Norway spruce and the laser equipment that they had access to (WoodEye, the same scanner as was used by Olsson et al 2013). They also developed a scheme to assess the 3D fiber orientation around knots. Moreover, similar scanning equipment and mapping functions for assessment of diving angle were adopted by Briggert et al (2016) and Kandler et al (2016) for studies on reconstruction of knots geometries within timber boards on the basis of identified knot surfaces.

Objectives and Limitations

The objectives of the present study are to 1) investigate the possibility of identifying the diving angle close to knots in Norway spruce timber through laser scanning using the tracheid effect, 2) determine the 3D fiber orientation within the entire board volume on the basis of information from tracheid effect scanning in combination with knowledge of how fibers grow around knots in trees in general, and 3) assess the possibilities of using the fiber orientation model to accurately calculate the local stiffness within the board. Thus, the first two objectives correspond to the establishment of a more detailed fiber orientation model of timber than the one that constituted the base for the grading method developed by Olsson et al (2013), whereas the third objectives is about assessment of how accurately this model can predict local stiffness of examined boards. The assessment corresponding to the third objective comprises both FE calculations and bending of boards in laboratory at which digital image correlation (DIC) is applied. This is developed in Methods and Equipment section.

A limitation of the study is that only side boards of Norway spruce, ie boards cut from a large distance to the pith, are examined. For such boards, the annual rings are relatively close to parallel with the wide surfaces and the direction of most of the knots is close to perpendicular to the wide surfaces of the boards, whereas the annual ring pattern and knot directions of center cuts present larger variations.

METHODS AND EQUIPMENT

Laser Scanning and the Industry Scanner WoodEye

For identifying fiber orientation on the basis of the tracheid effect, as described in Laser Scanning and the Tracheid Effect section, an optical scanner of make WoodEye was used. Such a scanner is available at Linnaeus University for research purposes and it has been used also in previous studies (eg Olsson et al 2013; Olsson and Oscarsson 2014; Briggert et al 2016). The installation includes conveyor belts, which feed boards in their longitudinal direction through the scanner at a maximum speed of about 450 m/min, which corresponds to a scanning speed that is frequently occurring at sawmill production. In the scanning process, all four longitudinal surfaces of a board are exposed to a row of laser rays. The row on each of the surfaces

is oriented in the transversal board direction. Because of the tracheid effect, each laser ray generates an elliptical dot on the board surface (Fig 1b-c). The major axis direction of each dot indicates the local fiber direction on the surface. This information is recorded by multisensory cameras when a board is passing through the scanner. The resolution of dot laser information in the longitudinal board direction is partly dependent on the sampling frequency of the cameras, but more important is the speed with which the board is fed through the scanner; the higher the speed, the lower the resolution. To achieve a high spatial resolution, the feed speed was in this investigation set to 75 m/min, which resulted in a longitudinal resolution of approximately 1.3 mm, ie the distance between two measurement points in the longitudinal direction of the board was 1.3 mm. In the transversal board direction, the spatial resolution is mainly determined by the design of the dot laser grid of the laser source. In industrial applications of the WoodEye scanner, a grid that results in a resolution of 4 mm is used and such a grid was also applied in this investigation, ie the distance between two measurement points in the transverse direction of the board was 4 mm. For the present investigation, a laser dot grid with a resolution of 1.3 $\times$ 4 mm was thus available. Data from both wide faces of the investigated boards were used for assessment of both in-plane fiber orientation and of fiber diving angles.

Dynamic Excitation and Weighing of Boards

For assessment of average MOE of boards an impact hammer, a microphone and fast Fourier transformation analyzer giving the resonance frequency of boards, and a balance giving the weight, were used.

Finite Element Analysis and Software

For assessment of local stiffness of examined boards, see objective 3 in Objectives and Limitations section, FE modeling and simulation of four-point bending were performed using the commercial software ABAQUS (from Dassault Systèmes, Vélizy-Villacoublay, France). In addition, the software MATLAB (from MathWorks Inc, Natick, Massachusetts USA) was used to calculate the fiber orientation information that was evaluated in this study.

Four-point Bending Test According to EN 408

To subject examined boards to bending, as a means to induce strains in the boards to be compared with strains according to FE calculation, four-point bending tests were carried out in accordance with the European Standard EN 408.

Digital Image Correlation and the System ARAMIS

The strains that arise in the physical boards when subjected to four-point bending were captured on both wide faces of the boards by means of DIC. For this purpose, two sets of an optical system of make ARAMIS (from Gesellschaft für Optische Messtechnik, Braunschweig, Germany) were used. The ARAMIS system is built on DIC and stereo vision techniques and is used to measure 3D displacements occurring on the surfaces of structures. Each system includes two cameras and digital images are recorded before and during loading. A measurement is implemented by taking images at a number of stages between which prescribed load increments are applied. By preparing the object surface with a stochastic spray pattern, the position of each conjugate pair of subpictures (called facets) in the two images taken by the dual cameras can be identified. Thus, the actual surface structure can be reconstructed. By repeating the same computation for all the load stages, the 3D coordinates for each facet are tracked and subsequently used to calculate displacements and strains. The results obtained were comparable with those from a FE analysis.

The 3D coordinates on both wide faces of each board were recorded with a spatial resolution of about 1.5 mm in both horizontal and vertical direction. Regarding accuracy of the measured 3D coordinates, it was about 0.01 mm in horizontal and vertical direction (x and y directions)

and 0.02 mm in direction out of the plane (z direction).

In the last 10 yr, DIC technique has been increasingly used in wood-related research (eg Sjödin et al 2006; Jeong et al 2009; Hu et al 2015). For further details of the system ARAMIS employed herein, see Oscarsson et al (2014).

MATERIAL

An original batch of 360 side boards of Norway spruce with dimensions 25 × 125 × 4800 mm was delivered to Linnaeus University from Södra Timber's sawmill in Torsås, located in the southeast part of Sweden. From this batch, 20 boards with larger knots were selected for investigation. Before testing, they were stored in a climate room at a temperature of 20°C and 65% RH for about 8 mo. After that, their average MC, determined using the so-called ovendry method described in EN 13183-1(2003), was 12.9% with a standard deviation (SD) = 1.0%. The corresponding average density was 506 kg/m^3 (SD = 40 kg/m^3).

The species of Norway spruce was chosen for reason of both convenience and continuity. Concerning the first reason, timber samples used in research carried out at Linnaeus University are mainly delivered from sawmills in the southeast part of Sweden, and since the bulk of sawn timber produced in this area is of Norway spruce, this species is easily supplied. As regard the second reason, Norway spruce was used for the development of the new strength grading method described in Strength Grading Based on Data of Fiber Orientation section. As the research presented in this paper is related to a further development of this method, Norway spruce was a choice of continuity.

As mentioned in Objectives and Limitations section, the present study only concerns side boards. This kind of product was chosen since the variation of annual ring pattern and knot directions is smaller in such boards than in center cuts, which means that the fiber orientation of side boards is easier to model.

Regarding the dimension of the test specimen, the 20 boards were to be subjected to four-point bending tests. Because of the slender cross-sectional dimensions of the boards, there was a risk of lateral instability occurring in the mid span during the bending tests. Such instability could be avoided by applying lateral supports between the two point loads. However, this was not an option in this case since the strain development on both wide surfaces of the mid span of each of the 20 boards was to be determined on the basis of displacements measured on these surfaces during the bending tests using two master-slave-connected DIC systems. Instead, the risk of lateral instability was eliminated by reducing the depth of the boards as well as applying lateral constraints outside of the loading points (see Fig 7a). By planing, the cross-sectional dimension was thus reduced to 24 × 95 mm. Since the mentioned four-point bending test requires a minimum span length of 18 times the board's depth, the length of the boards was decreased by crosscutting to 2000 mm. The planing and the saw cuts of each board were chosen such that the critical section, ie the assumed weakest section of the board, included a large traversing edge knot located in the middle of the mid span. Typical critical sections are shown in Fig 5f-g.

ESTABLISHMENT OF 3D FIBER ORIENTATION MODEL

The Introduction and Methods and Equipment sections comprised a description of laser scanning of boards for determination of the fiber orientation on surfaces. Below follows a more precise description of how to determine the diving angle, how to apply knowledge of fiber orientation on surfaces in a modeling and calculation scheme to determine location and direction of knots, and finally how to determine the fiber orientation including direction of the diving angle in relation to the position of the nearest knot. The modeling procedure presented in this section is mainly based on findings presented by Olsson and Oscarsson (2014).

Determination of the Diving Angle

The raw data from the scanning consisted of images of elliptic laser dots are shown in Fig 1b. In the present study, truncation at a fixed light intensity threshold value, in accordance with the default setting of the WoodEye machine, was applied to determine the directions and lengths of the main axes of the elliptic dots. Such axes are shown in Fig 1c. The angle between the direction of the longer axis and the edge of the board was interpreted as the local direction of the fibers in the plane of the investigated surface.

The length ratio between the main axes shown in Fig 1c was used to determine the value of the angle between the surface and the local fiber direction, also referred to as the diving angle. The following equation, which is based on principles presented in Simonaho et al (2004) and Olsson and Oscarsson (2014), expresses the assumed relationship between this ratio and the diving angle:

$$\beta = \frac{1}{2}\cos^{-1}\left(\left(\frac{r_1 + r_2}{2} - R\right)\frac{2}{r_2 - r_1}\right) \qquad (1)$$

Here, β is the value of the diving angle of interest, R is a shape factor that represents the length ratio between the two main axes of the elliptic laser dot, and r_1 and r_2 represent two constant threshold values of R. The parameter r_1 is a value below which β is set to 0° and r_2 is a value above which β is set to 90°.

Eq 1 was established on the basis of experimental data achieved from scanning of the 20 boards used in this investigation. The parameters r_1 and r_2 may be used for calibration, which could be needed since the interpretation of the light intensity and the length ratio of the elliptic laser dots may differ between different wood species and perhaps also between different scanners. Values employed in the current study were $r_1 = 0.54$ and $r_2 = 0.82$. These values were based on the condition that the diving angle calculated at a position close to the edge of a wide surface should be the same as the in-plane fiber direction at a nearby position on the adjacent narrow surface. Figure 3 shows the relationship between β and R as well as the significance of the parameters r_1 and r_2. To reduce the influence of measurement noise, the employed values of R in Eq 1 were averaged over surrounding areas of 5 × 5 mm^2. It should be noted that this choice had some significance for the adopted values of r_1 and r_2. If the averaging was done over a smaller or larger area, the values of r_1 and r_2 determined as explained would be somewhat different.

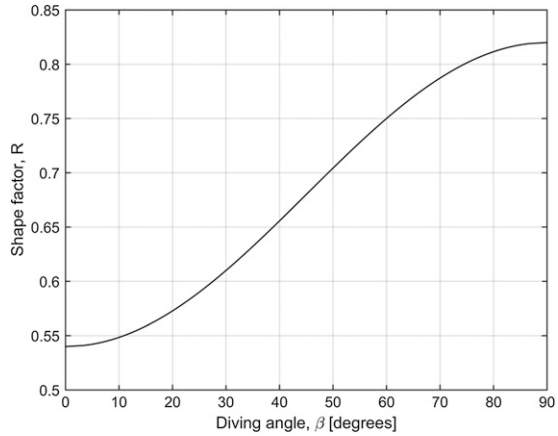

Figure 3. Relationship between the shape factor, R, and the value of the diving angle, β. The parameters r_1 and r_2 are used for calibration to experimental data.

Identification of Knots on the Wide Surfaces

The next step in the calculation scheme was to identify knot areas on the wide surfaces using the values of the diving angle. In this paper, a position on the wood surfaces where the diving angle was larger than 50° was interpreted as being within a knot. When a number of adjacent positions in longitudinal or transversal direction were all identified as being within a knot, it was assumed that these positions were parts of the same knot. After having identified knots as coherent areas an additional rule was applied—if two coherent areas were closer to each other than a certain distance, r_{crit}, they were assumed to be parts of the same knot. The distance r_{crit} was defined as

$$r_{crit} = \sqrt{A_1/\pi} + \sqrt{A_2/\pi} + r_{fix} \qquad (2)$$

where A_1 and A_2 are the areas of the two coherent knot areas and r_{fix} is a fixed distance. The two coherent knot areas were then considered as a single knot of size $A_1 + A_2$. In this investigation, r_{fix} was set to 20 mm. Finally, knot areas being smaller than 10 mm^2 were disregarded.

Determination of Pith Location of the Log

After knots were identified with respect to size and position on the wide faces of the board, a criterion was employed to assess whether knot surfaces visible on opposite wide faces belonged to the same knot. When the distance in the *xy* plane between the centroid of a knot on one surface and the centroid of a knot on the other surface was smaller than 24 mm, it was assumed that the two knots (ie visible knot areas) were parts of the same knot. The employed critical distance of 24 mm corresponds to the thickness of the board. For each knot being visible on both the two wide faces, the pith of it was determined as a straight line going through the centroids of the two knot areas. Thus, the pith for each such knot was determined with respect to position and direction.

When the direction of the pith of each knot was established as shown in Fig 4b–c, the pith of the log was determined as follows: 1) the angle, θ_i, between each pair of piths of the knots in the *xz* plane were calculated; thereafter the median, θ_{med}, of all those angles were determined; (2) for each pair of knot piths where $\theta_i \geq \theta_{med}$, an intersection point was calculated with respect to *x* and *z* coordinates (The reason why intersection points derived for pairs of knot piths with smaller angles in between were disregarded was the large sensitivity to errors in those cases, ie small errors in small angles give large errors in the corresponding calculated intersection point.); the average *x* and *z* coordinates of the intersection points were found and regarded as the log pith location in the *xz* plane; and (3) based on information of the identified log pith location, the root/top end of the log was then identified through studying the *y* coordinate of the centroids of each knot area on the two wide faces. For the example shown in Fig 4, it is found that the pith of the log is located above the top surface of the board sketched in panel a, and the end of the board with zero *y* coordinate is the root end of the log. This is consistent with the fact that branches in Norway spruce in most cases grow upward from the pith toward the bark. As the reader may have noticed, the procedure requires that a board being scanned contains a number of knots that are visible on both wide surfaces.

Knots only identified on one wide face were assumed to be directed, in the *xz* plane, toward the pith of the log and, in the *yz* plane, in the same direction as the median direction of the knots being visible on both wide faces, ie the median angle to the *y* axis of the lines in Fig 4c. The fiber orientation within surfaces

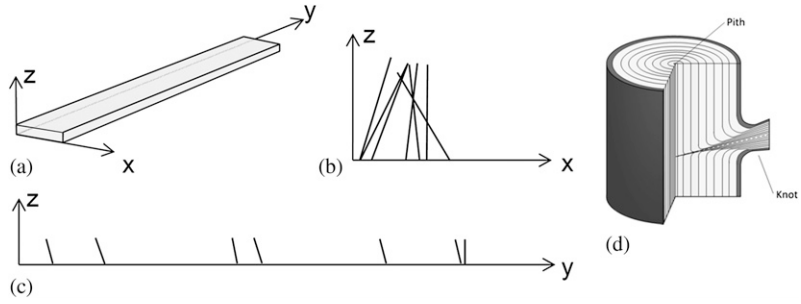

Figure 4. (a) A sketch of a board, along with a three-dimensional Cartesian coordinate system, (b) the orientation in the *xz* plane of the identified piths of knots/branches, (c) the orientation in the *yz* plane of the piths of the knots, and (d) a sketch showing the growth property of trees and a branch/knot pointing toward the pith of the log (images a-c originate from Olsson and Oscarsson 2014).

identified as knots are assumed to be parallel to the pith of the knot, ie the fiber orientation within knots, originally determined on the basis of the tracheid effect, was replaced.

Determination of Correct Sign of the Diving Angle

The fiber direction in the vicinity of a branch in a tree gradually changes from being, at a large distance from the branch, close to parallel to the pith of log to become, within the branch itself, close to parallel to the pith of the branch. Therefore, fibers below a branch are directed in a quite different way than fibers above a branch, in a sense that the fiber orientation is more or less symmetric about the pith of the branch as shown in Fig 5h. The last step of modeling thus consisted of assignment of a *sign*, positive or negative, to the diving angle which until now have only been determined with respect to an absolute value. For each position on a wide

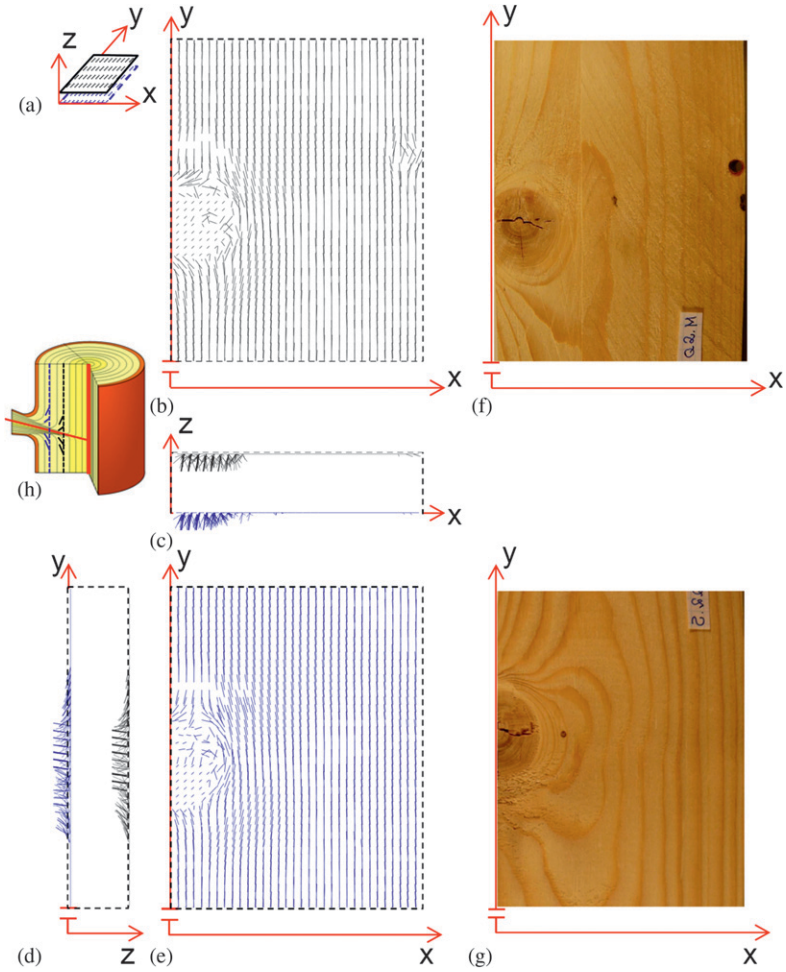

Figure 5. Identified three-dimensional fiber orientation on the two wide faces of a part of an examined board (no. B002) including a knot; (a) schematic perspective image, (b) fiber orientation of the top surface projected on the *xy* plane, (c) fiber orientation of both surfaces projected on the *xz* plane, (d) fiber orientation of both surfaces projected on the *yz* plane, (e) fiber orientation of the bottom surface projected on the *xy* plane, (f) and (g) photographs of the two wide faces (the picture in [g] is a vertically mirrored image of the original photograph), and (h) a schematic sketch showing that the fiber orientation in the vicinity of a knot is dependent on the position in relation to the knot.

surface the closest knot was identified. If then, when assuming a positive sign of the diving angle of the fibers in a certain position, the end of the fibers closer to the pith of the log had a longer distance to the pith of the knot than what the other end of the fibers had, the positive sign was preserved. Otherwise, it was changed to a negative sign. This rule was applied to the fiber orientation visualized for a part of a board shown in Fig 5 in which panels b and e show fiber orientation on the two wide faces of a 130-mm-long part of a board including a knot. Figure 5d shows the fiber orientation on the two wide faces in a sideway's view. In Fig 5h, the same board and view is indicated by blue and black lines. Note that the fibers are directed as can be expected with respect to the log pith and the knot/branch pith. Figure 5f-g show photographs of the two wide surfaces of the part of the board. Note, however, that the image shown in Fig 5g is a vertically mirrored version of the photograph actually taken of this surface.

Establishment of a Full-field Fiber Orientation Model

When the surface fiber orientation was established, resulting in such information as is visualized in Fig 5, the full-field data within the entire volume of the board were created simply through linear interpolation in the z direction, ie as

$$\mathrm{f}_{\mathrm{xy}}(x_i, y_i, z) = \phi_{\mathrm{xy}}(x_i, y_i, 0) \cdot \frac{t - z}{t} + \phi_{\mathrm{xy}}(x_i, y_i, t) \cdot \frac{z}{t} \qquad (3)$$

and

$$\phi_{\mathrm{diving}}(x_i, y_i, z) = \phi_{\mathrm{diving}}(x_i, y_i, 0) \cdot \frac{t - z}{t} + \phi_{\mathrm{diving}}(x_i, y_i, t) \cdot \frac{z}{t} \qquad (4)$$

where φ_{xy} is the angle in xy plane and $\varphi_{\mathrm{diving}}$ is the diving angle, x_i and y_i are coordinates of a position i on a wide face where the fiber orientations are known, z is the coordinate in the direction perpendicular to the xy plane, and t is the thickness of the board (here 24 mm).

ASSESSMENT OF THE FIBER ORIENTATION MODEL

The fiber orientation model should be useful for engineering analyses, such as the basis for accurate FE models for assessment of stiffness of timber. Therefore, such an application is presented in this section for the purpose of evaluation. FE models of boards with the fiber orientation determined as described in *Establishment of 3D Fiber Orientation Model* section were established whereupon pure edgewise bending was simulated and the resulting strains were calculated. Moreover, corresponding laboratory tests were performed and strain fields that were compared with those from the FE simulations were determined on the basis of 3D displacement measurements using DIC technique.

FE Model and Calculation of Strain Fields

As described in Method and Equipment section, the FE modeling was performed using the commercial software ABAQUS in which 3D models of wooden boards using eight-node linear hex brick elements were created. The material was defined as linear elastic and transversely isotropic, with material properties with respect to the local directions as presented in the column labeled "Nominal values" in Table 1. A distinction was, thus, made between stiffness in the fiber direction and the across fiber directions but not between the tangential and the radial direction. The MOE in the fiber direction E_l was set in accordance with a longitudinal dynamic MOE assessed experimentally for the board investigated as described in Olsson et al (2013) and the other stiffness properties were set based on their ratios to the E_l, which were assumed to be representative for Norway spruce.

The identified fiber orientations on two wide faces of the boards were used as modeling input data. The data supplied consisted of five parts, x, y, and z coordinates and two angles, φ_{xy} and $\varphi_{\mathrm{diving}}$, for each position on the two wide

Table 1. Material parameters adopted in the finite element model.

Parameter	E_l (MPa)	E_t (MPa)	E_r (MPa)	ν_{tl}	ν_{tr}	ν_{lr}	G_{tl} (MPa)	G_{tr} (MPa)	G_{lr} (MPa)
Nominal value	14,349	478	478	0.015	0.45	0.45	897	45	897
Reduced stiffness	143.49	4.78	4.78	0.015	0.45	0.45	8.97	0.45	8.97

surfaces. As a preparation for a FE analysis using the software ABAQUS, a so-called user subroutine for this software was developed and used for reading the input data, achieving full-field data by means of interpolation using Eqs 3-4, and defining the local material direction correspondingly by direction cosines using the two angles. As a result, the fiber orientation determined by means of scanning could be conveniently adopted in the FE model.

Figure 6a illustrates the loading case and the part of the board modeled in ABAQUS including an edge knot. Figure 6b shows the FE model in which the elements are mainly colored in blue and red. The FE models employed had an element size of 1.5 mm in x and y direction and 3 mm in z direction. The red zone in the FE model is five elements, ie 7.5 mm, wide in y direction. As can be seen in the photographs of Fig 5f-g, there is a crack going through the knot at the edge of the board. Therefore, the FE model was prepared such that the elements marked red may be assigned either the nominal values in the material direction just as the material in all other elements of the model, or the "Reduced stiffness" defined in Table 1 to mimic the locally reduced stiffness caused by the crack.

The aim of the FE model was to simulate a load case of pure bending where the edge that included the knot was subjected to tension. The FE analysis did not aim at studying the crack propagation or the localized strain concentrations close to the crack, but rather the influence of the grain deviation on the overall displacement and strain fields. Calculated results were displacements and strains in different directions. Of course, strains could be visualized directly in ABAQUS, but here the software MATLAB was used instead since using the same software for visualizing strains calculated on the basis of the FE simulation and strains calculated on the basis of displacements measured during the corresponding laboratory test facilitates the comparison.

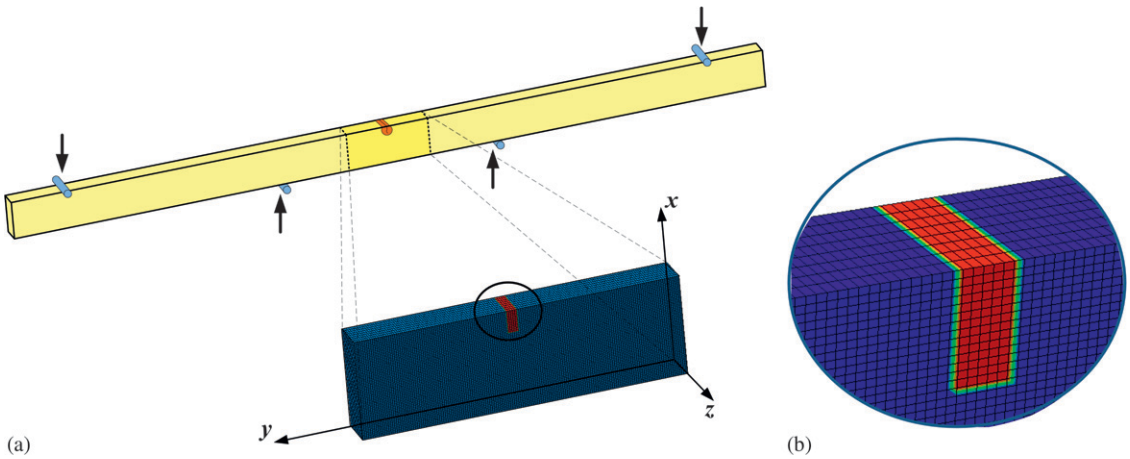

Figure 6. Illustration of a finite element (FE) model of a wooden board including an edge knot. (a) It shows the four-point bending load case and the FE model of a part of the board including the edge knot. (b) An enlarged image showing the mesh near the edge knot. The FE model is prepared such that the elements marked red in (b) can be assigned either the "Nominal value" or a "Reduced stiffness" (Table 1).

The employed element mesh was uniform, ie no refinement of the element mesh or adoption of element edges to the knot interface was performed. The simple mesh employed would be inadequate for the purpose of predicting, eg crack propagation but it was sufficient to calculate a strain field to compare, qualitatively, with strain fields from DIC measurements covering a rectangular areas of about 100 × 200 mm. Different, coarser, and finer meshes were evaluated to ensure that the element size finally employed was sufficient fine to represent the strain field on the level on which the evaluation and comparison were carried out.

Displacement Measurement and Strain Field Determination

As described in Methods and Equipment section, DIC were used to follow the development of strains on both wide faces of a section of the loaded board. The detailed setup of the four-point bending test, which results in a pure bending moment over a 570-mm-long part of the board between the two point loads, is displayed in Fig 7a. The edge knots in the middle of the boards were placed at the tension side, ie the upper edge as shown in Fig 7a. Figure 7b shows the same test setup from a different view showing also the setup of the DIC systems by which full-field data can be recorded for strain calculation. As shown in the figure, the DIC systems placed on the two sides of the board were referred to as a master and a slave system, respectively. The two systems were both focused on the middle part of the board between the loading points, which ensured that the edge knot was covered from both sides.

The 3D coordinates on both wide faces of each board were recorded as functions of the load level by the DIC systems with the spatial resolution and accuracy that are given in Methods and Equipment section. The bending test was run until ultimate failure and the force-displacement time history was recorded. The two DIC systems worked with triggers set by the master system to ensure that the two systems acted simultaneously. Images and load signals were sampled approximately at every 15 s time increment and at every 100 N load increment. Thus, there was for each board assessed a load-displacement curve, eg as shown in Fig 8, with data available at each position marked with a small or a larger dot. The stress levels given at the stages indicated with larger dots in Fig 8 are the maximum stresses in the board, calculated on the basis of beam theory and assuming a constant stiffness of the material over the board cross section. In the

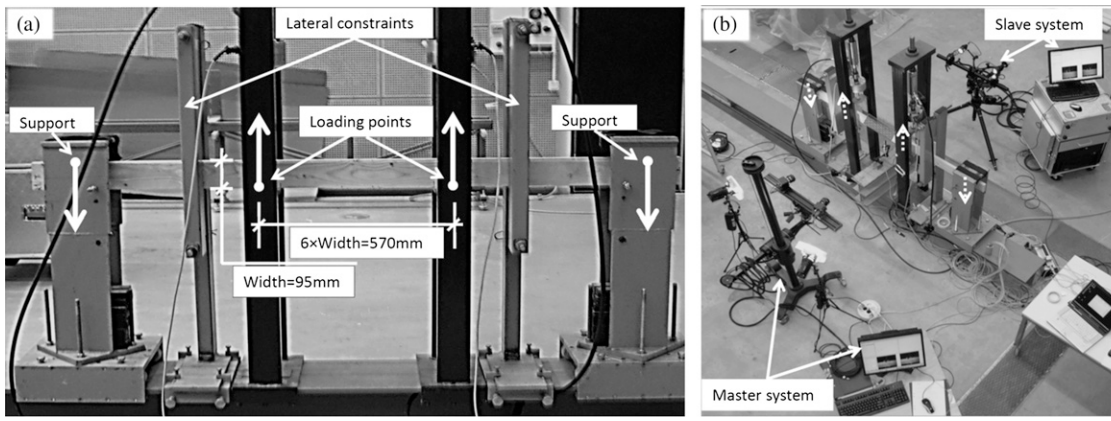

Figure 7. Displacement measurement setup: (a) bending test setup in a perspective from one side and (b) overview of the setup showing the two ARAMIS systems, ie one set of cameras and computer/screen on one side of the board (measured by the master system) and another set of camera and computer/screen on the other side of the board (measured by the slave system).

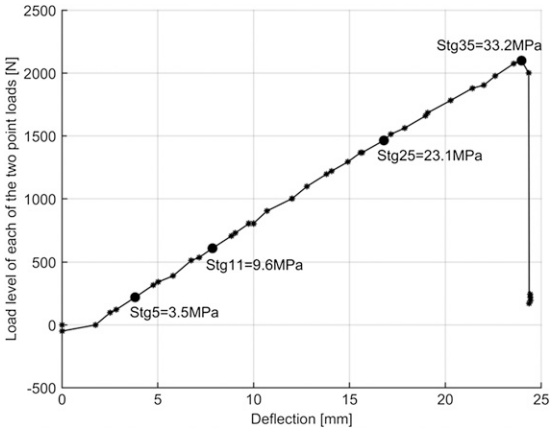

Figure 8. Load-displacement curve of one of the investigated boards (no. B002). The black markers on the curve represent the load stages implemented in the measurements, whereas the bigger ones represent the stages chosen to present the strain fields in the result section; the corresponding nominal stress level for those stages are shown as well.

following sections, such stresses are referred to as nominal stresses for the corresponding load levels. The output data of the measurement were full-field 3D coordinates of the two wide faces covered by the DIC systems as function of the applied load. The data were used to calculate displacements and strains in MATLAB using self-developed routines.

RESULTS AND DISCUSSION

In this section, results with respect to fiber orientation and strains in a board subjected to bending are presented. For comparison, and for evaluation of the ability of the fiber orientation model, strains were calculated on the basis of both laboratory tests and simulation results from the FE modeling. Detailed results are presented only for one board, but this one is representative for the board sample investigated.

Results of the Fiber Orientation Model

An example of results regarding fiber orientation is shown in Fig 5. The fiber orientation that can be seen in the *xy* plane, see Fig 5b and e, follows the longer main axes of the elliptic laser dots achieved on the surface during scanning. The ratio, R, that determined the diving angle, β, affects the graphical representation of the result in the *xy* plane in the sense that the length of the lines representing the local fiber orientation are shorter in positions where the diving angles are substantial, which are in the area of the knot. In Fig 5c and d showing the determined fiber orientation in the *xz* plane and in the *yz* plane, respectively, the effect of large values of R, giving large diving angles within and in the surroundings of the knot, is very clear. The results show that the calculated orientation of fibers in the vicinity of a knot agree well with what is known about the fiber orientation around or at some distance to knots in general. The rule applied for determining the sign of the diving angle also works well. The correct diving angle can be assessed close to the corners between surfaces, since the in-plane fiber orientation on one of the surfaces, close to the corner, can be regarded as the correct diving angle of the adjacent surface close to the edge having a 90° angle to the other surface. Of course, a thorough calibration with respect to the relation between R and β should be carried out for each scanner to be used for assessment of diving angles.

In the narrow transition zone between knot and clear wood the true fiber pattern is intricate (Shigo 1986) since some fibers integrate with the knot, whereas others grow around it. The information from the laser scanning used was too coarse to capture the distinction between the two different fiber orientations in the transition zone. When the proposed fiber orientation modeling scheme is used for calculations of, eg linear elastic behavior of entire boards, or part of boards, with knots this limitation is probably negligible. However, the fiber orientation model should be used with caution when, eg a fracture mechanics approach is used for assessment of strength of a board in bending or tension, since the crossing fibers around a real knot means a reinforcement that is not captured accurately by the fiber orientation model as derived in this paper. Grain-flow analogy that have been presented in the past (eg Philips et al 1981; Guindos

and Guaita 2013) gives a fair resemblance to the actual fiber orientation of the fibers that flow around a knot but not of fibers that integrate with the knot. Thus, such models also suffer from the same limitations.

Strain Distribution from DIC

Figure 9 shows calculated normal longitudinal (*y* direction) strains on the wide surfaces of the same board as shown in Fig 8. The strains are here averaged over areas of 3 × 3 mm^2 and are shown for load stages 5, 11, 25, and 35, which are all within the linear range of the load-displacement curve. These load stages are marked with larger dots in Fig 8. In Fig 9, strains corresponding to the pith side of the board (measured by the master ARAMIS system) for ascending load levels are shown by images (a), (c), (e), and (g) and the bark side of the board (measured by the slave ARAMIS system) are shown by images (b), (d), (f), and (h).

As expected, the pattern in the clear wood show tension strains on the upper parts of the board and compression strains on the lower parts. These strains seem to increase linearly with increased load level. On a more detailed level, it is possible to see more complicated strain patterns. Already at the lowest load level, large spurious strains are identified on both surfaces

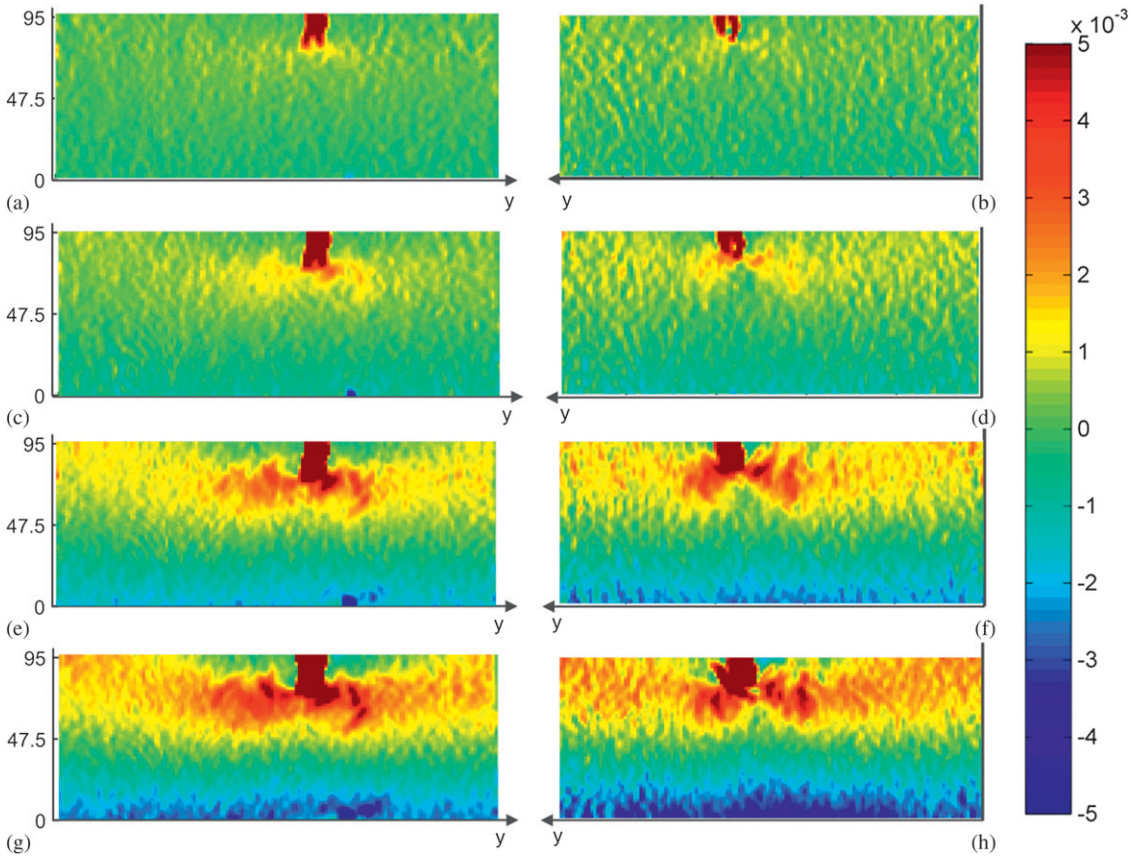

Figure 9. Normal strain distribution, for board no. B002, in longitudinal board direction (*y* direction) at four different load levels, ie stages 5, 11, 25, and 35, which are shown in Figure 8. The strains at ascending load levels on the pith side of the board (measured by the master ARAMIS system) are shown by images (a), (c), (e), (g), and similarly the strains on the bark side of the board (measured by the slave ARAMIS system) are shown by images (b), (d), (f), and (h).

of the edge knot, which is due to the initial crack in the knot. Since the loaded board was examined by DIC with a limited resolution, the crack opening is interpreted as a zone of some width with large strains. In reality, however, there are no strains in the unloaded material that borders the crack. The opening of the crack increased with increased load level and at higher load levels real strains in the material in the surrounding of the knot emerged, as can be seen in Fig 9c-h. On the strain plots that correspond to the higher load levels, it can be seen that large positive strains appear under the knot and spread longitudinally and slightly upward. Of course, such a strain pattern is expected in a board with either a crack or a knot placed on the edge on the tension side. Note, however, that there is also some strain concentrations in the compression zone close to the lower edge and slightly to the right of the knot in Fig 9c, e, and g. When studying the pith side of the board, which is shown in Fig 5f, it can be seen that there is a small hole after a dead knot in this position.

Comparison of Simulation and Laboratory Results

The laboratory tests were performed to give a basis for evaluation of the performance and accuracy of the FE models in which the fiber orientation information was included. Figure 10 shows normal longitudinal (*y* direction) strains determined in different ways on the wide surfaces of the board. Figure 10a and b displays strains based on the FE model and simulation with nominal material stiffness properties (cf. Table 1), ie without considering the initial crack in the knot, Fig 10c and d shows DIC results for load stage 35, ie the same strains as displayed in Fig 9g and h. Figure 10e and f exhibits strains determined by means of the FE model with reduced material stiffness, ie with

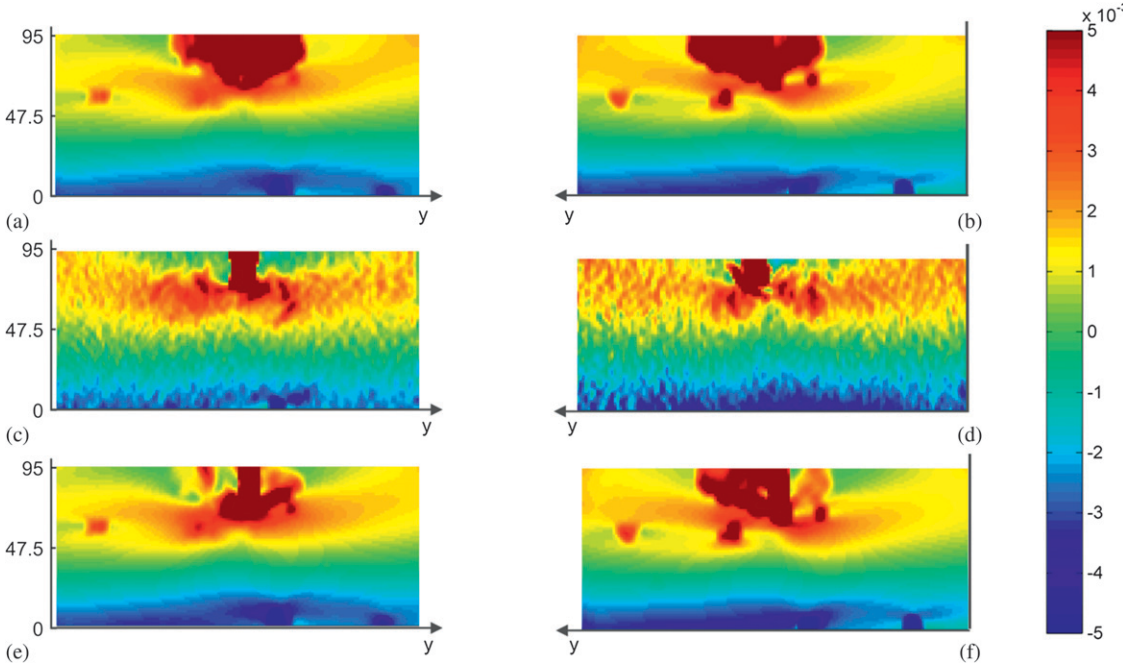

Figure 10. Normal (*y* direction) strains valid for board no. B002 corresponding to a nominal stress level of 33.2 MPa at the board edges: strains derived from (a-b) an finite element (FE) model with nominal material stiffness properties, (c-d) digital image correlation results, and (e-f) the FE model with reduced material stiffness, ie with consideration to the initial crack in the knot. Left images, (a), (c), and (e), display strains for the pith side/master surface. Right images, (b), (d), and (f), display the strains for the bark side/slave surface.

consideration of the initial crack in the knot. The strains calculated with the FE models are valid for the same load level as those originating from the DIC measurement, ie two point loads of 2099 N resulting in a nominal stress level of about 33.2 MPa at the outmost fiber of the board.

Comparing the different strain plots of Fig 10, there is an obvious resemblance between the results from the FE models based on the fiber orientation model and the result from DIC measurement, both regarding the strain pattern and the strain levels. The FE model that ignored the initial crack in the knot (Fig 10a and b) indicates large positive strains over an area slightly larger than the knot itself. Of course, this is due to the low longitudinal stiffness in positions where fibers are directed perpendicularly to the longitudinal direction of the board. Thus, locally, in the knot itself, this model give a different strain pattern compared with the other strain plots. In this respect, the FE model that takes the crack into account (Fig 10e and f) show better agreement with the DIC results (Fig 10c and d). Note, however, the crack only caused a local effect. Apart from an area only slightly larger than the knot itself, there is hardly any difference between Fig 10a-b and Fig 10e-f. Both the FE models and the DIC results show concentrated positive strains just below the knot, both to the left and to the right of it. Also, the concentrated negative strain on the compression edge of the board, slightly to the right of the knot on the pith side/master surface (caused by the hole visible in Fig 5a) could be distinguished in both FE simulation and DIC results. However, the FE models also show a few local strain concentrations that, far away from the knot, are not shown by the DIC results. These could be explained by apparent fiber deviations detected in single measurement positions by means of

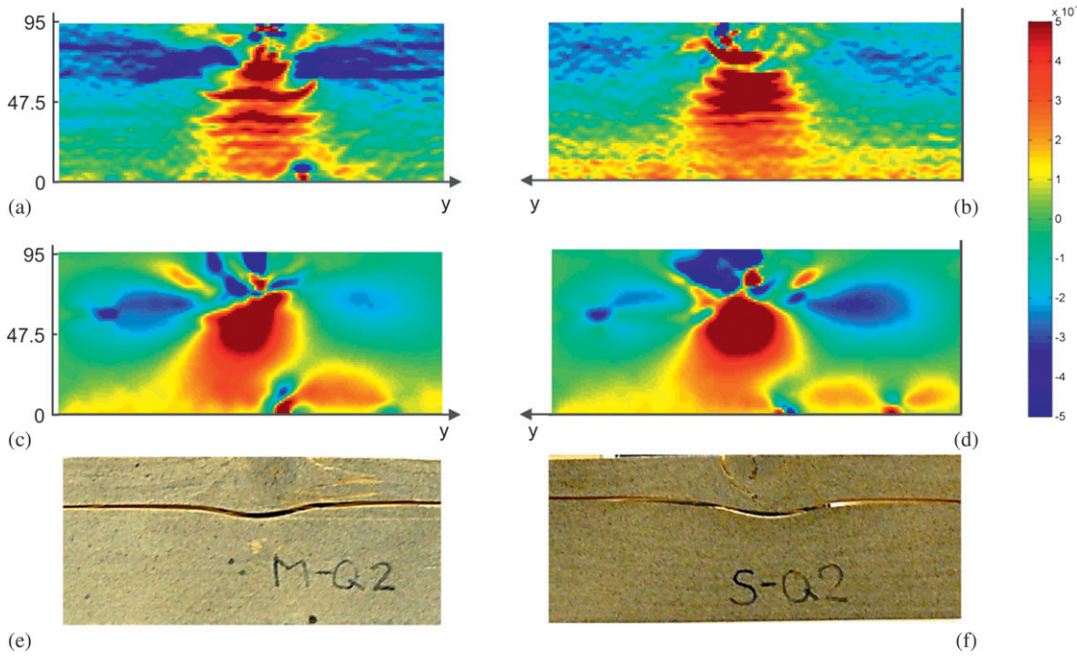

Figure 11. Transversal (*x* direction) normal strains valid for board no. B002 corresponding to a nominal stress level of 33.2 MPa at the board edges: strains derived from (a-b) the digital image correlation results, (c-d) the finite element model with reduced material stiffness, ie with consideration to the initial crack in the knot, and (e-f) photographs of the evaluated part of the board after ultimate failure. Left images, (a), (c), and (e), display results for the pith side/master surface. Right images, (b), (d), and (e), display the results for the bark side/slave surface.

the dot laser scanning. A chip or some shavings on one of the board surface might be the cause and, since a single laser dot represented a width of 4 mm in the direction perpendicular to the longitudinal direction of the board and it should be recalled that linear variation is assumed between the fiber angles of the two wide surfaces, this may be enough to explain the small spurious strain concentrations.

Figures 11 and 12 show normal strains in the transversal board direction (x direction) and shear strains. Figure 11c-d as well as Fig 12c-d show strains calculated on the basis of the FE model with reduced material stiffness, ie with consideration to the initial crack in the knot, whereas Fig 11a-b and Fig 12a-b exhibit strains based on the DIC results. As for the normal strains in longitudinal direction there is, both for transversal normal strains and for shear strains, an obvious resemblance between the results from the FE modeling and the result from the DIC. Regarding transversal normal strains, see Fig 11, large positive strains appeared just beneath the knot on all the plots. Consequently, bending tests of the investigated 20 side boards, each including a traversing edge knot on the tension side, the failure mode of each board included development of a longitudinal traversing crack beneath the knot. The crack propagated along the fiber direction (see Fig 11e-f) on both sides of the traversing knot. It should be noted that after the occurrence of the longitudinal crack, the ensuing ultimate failure occurred for almost all of the boards as a tension failure in the narrow strip that appeared between the mentioned crack and the tension edge (see Fig 11e-f).

Figure 11a-b shows a striped pattern in the zone of large positive strains beneath the knot. It corresponds to the annual ring pattern on the board. Naturally, there is no corresponding pattern in the strains calculated with the FE model, see Fig 11c-d, since the FE model did not consider inhomogeneity in the material on the level of annual rings. The small hole from the dead knot close to the lower edge of the board, somewhat to the right of the big knot on the upper edge, caused a strain concentration both on the transversal normal strain plots and on the shear strain plots in a way that corresponded to what was noticed on the longitudinal normal strain plots shown in Fig 10.

CONCLUSIONS

A modeling scheme for 3D fiber orientation of the entire volume of side boards of Norway

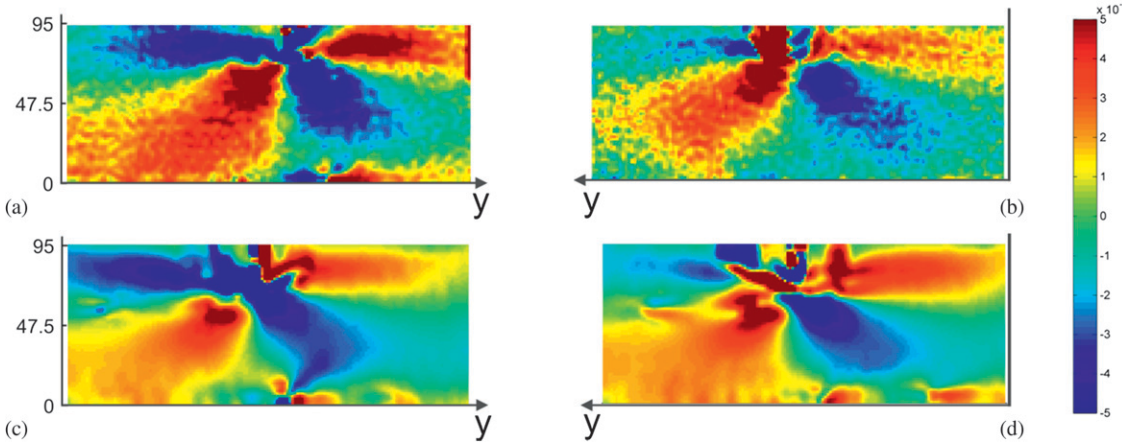

Figure 12. Shear strains valid for board no. B002 corresponding to a nominal stress level about 33.2 MPa at the board edges: strains derived from (a-b) digital image correlation results and (c-d) the finite element model with reduced material stiffness, ie with consideration to the initial crack in the knot. Left images, (a) and (c), display strains for the pith side/master surface. Right images, (b) and (d), display the strains for the bark side/slave surface.

spruce, based on data from dot laser scanning and utilization of the tracheid effect, was presented, as well as an applied study of the strain distributions in the boards exposed to four-point bending.

The in-plane and diving angles of fiber directions were determined using the tracheid effect by making use of the ovality of laser dots on the wood surface. Knot areas can be identified by means of the diving angles since the fiber orientation within a knot deviates substantially from the fiber orientation in clear wood. In the modeling scheme, the fiber orientation within knots simply followed the direction of the branch/knot. The 3D fiber orientation derived in clear wood areas around knots seemed to be in fair agreement with the actual fiber orientation on such surfaces. However, the data from scanning were too coarse to give detailed information of the fiber orientation in the narrow transition zone between knots and clear wood where, in reality, some fibers integrate with the knot, whereas others grow around it.

The fiber orientation models established were integrated with FE models of boards using the software ABAQUS. The models were used to simulate four-point bending tests of side boards with traversing knots located at the edge on the tension side. The same boards as evaluated and modeled with respect to their individual fiber orientation in 3D were also tested in four-point bending in laboratory and strains on the wide faces were calculated at different load levels using DIC technique, which enabled comparison with strains calculated on the basis of the FE models including the fiber orientation information. Comparisons of strain fields, ie normal strains in longitudinal and transversal board direction and shear strains, from measurements and simulations, respectively, showed close agreement regarding both strain patterns and strain levels. The large positive normal strains that occurred beneath the traversing edge knot and in a direction perpendicular to grain were well captured by the FE models. Also, small defects in the wood, eg a very small hole on one of the wide faces close to the edge on the compression side, caused local strain concentrations that were clearly detectable on the strain plots based on both the DIC measurements and the simulations.

In conclusion, the modeling approach presented for the 3D fiber orientation of boards showed promising results. It can be used for accurate calculations of strain fields but at its current degree of spatial resolution, the approach taken here is not capable of capturing the strain concentrations at crack tips. Thus, further development is needed before fracture mechanics calculations on the basis of the fiber orientation model are performed. In addition to the limited spatial resolution, caution must be taken in applying the model at its current state of development in situations that would suggest cracks crossing the transition zone between a knot and clear wood, since the fiber orientation model does not capture the reinforcing, crossing fibers that are located in the transition zone between knots and clear wood.

Further work would be to 1) make the modeling scheme more general, ie to make it able to handle boards also from the center part of the log and not only side boards. Recent work presented by Briggert et al (2016) contributes significantly in this direction, 2) evaluate the usefulness of the this fiber orientation models for improvement of the accuracy of the grading method presented by Olsson et al (2013), 3) address the fiber orientation in the transition zone between knots and clear wood, and 4) develop it and apply it for prediction of strength on the basis of crack propagation and failure modes of timber. An alternative to predicting the detailed fiber orientation in the transition zone can be to adapt stiffness, strength, and fracture mechanics parameters locally, so as to reflect the possible reinforcing effect of the transition zone in applied strength analyses. A recent example of such an approach is outlined in Jockwer et al (2015).

REFERENCES

Briggert A, Olsson A, Oscarsson J (2016) Three-dimensional modelling of knots and pith location in Norway spruce

using tracheid-effect scanning. Eur J Wood Wood Prod 74:725-739.

Cramer SM, Goodman JR (1983) Model for stress and strength prediction of lumber. Wood Fiber Sci 15(4): 338-349.

EN 13183-1:2003 Moisture content of a piece of sawn timber—Part 1: Determination by oven dry method.

EN 14081-2:2010 + A1:2012 Timber structures—Strength graded structural timber with rectangular cross section – Part 2: Machine grading; additional requirements for initial type testing.

Foley C (2001) A three-dimensional paradigm of fibre orientation in timber. Wood Sci Technol 35:453-465.

Foley C (2003) Modelling the effect of knots in structural timber. Doctoral thesis, Division of Structural Engineering, Lund University, Lund, Sweden.

Goodman JR, Bodig J (1978) Mathematical model of the tension behavior of wood with knots and cross grain. Proc First Int. Conf. on Wood Fracture. August 14-16, Banff, Alberta.

Guindos P, Guaita M (2013) A three-dimensional wood material model to simulate the behavior of wood with any type of knot at the macro-scale. Wood Sci Technol 47:585-599.

Hackspiel C (2010) A numerical simulation tool for wood grading. PhD thesis, Vienna University of Technology, Vienna, Austria.

Hu M, Johansson M, Olsson A, Oscarsson J, Enquist B (2015) Local variation of modulus of elasticity in timber determined on the basis of non-contact deformation measurement and scanned fibre orientation. Eur J Wood Wood Prod 73:17-27.

Jeong YG, Zink-Sharp A, Hindman DP (2009) Tensile properties of earlywood and latewood from loblolly pine (*Pinus taeda*) using digital image correlation. Wood Fiber Sci 41(1):51-63.

Jockwer R, Serrano E, Gustafsson PJ, Steiger R (2015) Impact of growth characteristics on the fracture perpendicular to the grain of timber. 12th International Conference on Applications of Statistics and Probability in Civil Engineering, ICASP12, July 12-15, Vancouver, Canada.

Johansson C-J (2003) Grading timber with respect to mechanical properties. Pages 23-43 *in* S Thelandersson and HJ Larsen, eds. Timber engineering. John Wiley & Sons, Ltd, Chichester, UK.

Kandler G, Lukacevis M, Füssl J (2016) An algorithm for the geometric reconstruction of knots within timber boards based on fibre angle measurements. Construct Build Mater 124:945-960.

Lang R, Kaliske M (2013) Description of inhomogeneities in wooden structures: Modelling of branches. Wood Sci Technol 47:1051-1070.

Lukacevic M, Füssl J (2014) Numerical simulation tool for wooden boards with a physically based approach to identify structural failure. Eur J Wood Wood Prod 72: 497-508.

Mattheck C (1998) Design in nature: Learning from trees. Springer-Verlag Berlin, Germany.

Matthews PC, Beech BH (1976) Method and apparatus for detecting timber defects. U.S. Patent 3,976,384.

Olsson A, Oscarsson J (2014) Three dimensional fibre orientation models for wood based on laser scanning utilizing the tracheid effect. Proc World Conference on Timber Engineering, August 10-14, Quebec City, Canada.

Olsson A and Oscarsson J (2016) Strength grading on the basis of high resolution laser scanning and dynamic excitation: a full scale investigation of performance. Eur J Wood Wood Prod DOI: 10.1007/s00107-016-1102-6.

Olsson A, Oscarsson J, Serrano E, Källsner B, Johansson M, Enquist B (2013) Prediction of timber bending strength and in-member cross-sectional stiffness variation on the basis of local wood fibre orientation. Eur J Wood Wood Prod 71(3):319-333.

Oscarsson J, Olsson A, Enquist B (2014) Localized modulus of elasticity in timber and its significance for the accuracy of machine strength grading. Wood Fiber Sci 46(4):489-501.

Petersson H (2010) Use of optical and laser scanning techniques as tools for obtaining improved FE-input data for strength and shape stability analysis of wood and timber. Proc IV European Conference on Computational Mechanics, May 16–21, Paris.

Philips G, Bodig J, Goodman J (1981) Flow-grain analogy. Wood Sci Technol 14:55-65.

Shigo AL (1986) A new tree biology: Facts, photos and philosophies on trees and their problems and proper care. Eighth Printing, Shigo and trees, Durham, NC.

Simonaho S-P, Palviainen J, Tolonen Y, Silvennoinen R (2004) Determination of wood grain direction from laser light scattering pattern. Opt Lasers Eng 41(1):95-103.

Sjödin J, Serrano E, Enquist B (2006) Contact-free measurements and numerical analyses of the strain distribution in the joint area of steel-to-timber dowel joints. Holz Roh Werkst 64:497-506.

Soest J, Matthews P, Wilson B (1993) A simple optical scanner for grain defects. Proc 5th International conference on Scanning Technology & Process Control for Wood Products Industry, October 25-27, Atlanta, GA.